DOI: 10.1002/chem.200501594

High-Spin- and Low-Spin-State Structures of $[Fe(chloroethyltetrazole)_6](ClO_4)_2$ from Synchrotron Powder Diffraction Data

Eva Dova,*[a] René Peschar,[a] Makoto Sakata,[b] Kenichi Kato,[c] and Henk Schenk[a]

Abstract: The spin-crossover complex $[Fe(teec)_6](ClO_4)_2$ (teec = chloroethyltetrazole) exhibits a 50% incomplete spin crossover in the temperature range 300–30 K. Time-resolved synchrotron powder diffraction experiments have been carried out to elucidate its structural behavior. We report crystal structure models of this material at 300 K (high spin) and 90 K (low spin), as solved from synchrotron powder diffraction data by using Genetic Algorithm and Parallel Tempering techniques and refined with Rietveld refinement. During short synchrotron powder diffraction experiments (five minutes duration) two distinguishable lattices were observed the quantities of which vary with temperature. The implication of this phenomenon, that is interpreted as a structural phase transition associated with the high-to-low spin crossover, and the structural characteristics of the high-spin and low-spin models are discussed in relation to other compounds showing a similar type of spin-crossover behavior.

Keywords: iron · spin crossover · structure elucidation · X-ray diffraction

Introduction

Spin crossover is the phenomenon that external influences (for example, temperature, light, or pressure) can change the spin state of an atom, thereby changing the total magnetic moment of the compound.[1–3] Spin crossover may find potential application, for example, in temperature sensors, in various types of molecular-based displays, and in information storage and retrieval.[1,4–9] A wide range of spin crossover has been observed experimentally, for example, gradual complete, two-step transitions, incomplete transitions with a residual high-spin (HS) species at low temperature, and hysteresis loops.[10–13]

[a] Dr. E. Dova, Dr. R. Peschar, Prof. Dr. H. Schenk
University of Amsterdam, Faculty of Science
van't Hoff Institute for Molecular Sciences
Laboratory for Crystallography
Valckenierstraat 65, 1018 XE, Amsterdam (The Netherlands)
Fax: (+31) 20-525-6940
E-mail: eva@science.uva.nl

[b] Prof. Dr. M. Sakata
Department of Applied Physics, Nagoya University
Nagoya 464–8603 (Japan)

[c] Dr. K. Kato
Japan Synchrotron Radiation Research Institute
Hyogo, 679–5198 (Japan)

Most of the studies of spin crossover have concentrated on iron(II) compounds.[14,15] Thermal spin crossover in coordination compounds of the form $[Fe(alkyltetrazole)_6](X)_2$ (with $X = BF_4^-$, ClO_4^-) were first described by Franke.[16,17] On the basis of magnetic susceptibility measurements, it was discovered that the 1-methyltetrazole (mtz) and the 1-ethyltetrazole (etz) complexes have a large residual of high-spin Fe^{II} ions at low temperature, 50% for the mtz complexes and 33% for the etz complexes. Crystal-structure determination of those complexes[18–19] revealed the Fe atom to be positioned at two crystallographically inequivalent sites in the unit cell, n_A and n_B. Because of the difference in the ratio n_A:n_B, 1:1 and 2:1 in the mtz and etz complexes, respectively, the large HS residue has been explained by assuming that the Fe atoms at site n_B remain in the HS state at all temperatures, while those at site n_A undergo a temperature-dependent spin transition.

The spin-crossover behavior of $[Fe(teec)_6](ClO_4)_2$ is similar to that of $[Fe(mtz)_6]X_2$, ($X = BF_4^-$, ClO_4^-), a single-step spin crossover of around 50% of the Fe^{II} ions. Magnetic susceptibility data of $[Fe(teec)_6](ClO_4)_2$ revealed that, when cooling once to low temperature (10 K), 50% of the Fe^{II} atoms remained in the HS state, while according to ^{57}Fe Mössbauer spectroscopy this percentage was lower (almost 20%). Additional ^{57}Fe Mössbauer spectroscopy experiments pointed out that by repeated cycles of cooling and heating

the percentage of the high-spin species at low temperature could be reduced virtually to zero.

Because of their similarity in spin-crossover behavior, it has been assumed that also $[Fe(teec)_6](ClO_4)_2$ has two different Fe^{II} sites n_A and n_B, with site n_A being associated with the change from HS to low spin (LS) between 235 K and 150 K, with $T_{1/2}=178.5$ K.[20,21] The high percentage of Fe^{II} ions remaining in the HS state as the temperature decreases has been attributed to the presence of a Fe^{II} site n_B that presumably does not undergo a spin-crossover.

To analyze the incomplete SCO in $[Fe(teec)_6](ClO_4)_2$ in more detail, synchrotron radiation powder data (SRPD) were collected at several temperatures in the range 300–90 K and over two different time scales, five minutes (scan data) and one hour (long-term data). For the long-term SRPD sets at 300 K (HS) and 90 K (LS) the corresponding crystal structures have been determined.

Results

Scan versus long-term data: The diffraction patterns of the scan measurements (Figure 1) show a remarkable evolution as the temperature decreases. Within the temperature range 300–180 K, the patterns change quite gradually and only a lattice contraction seems to occur. However, below 170 K, and in almost all regions of the patterns, reflections that were initially present at 300 K start to fade while new diffraction peaks appear. For example, below 150 K, very close to the strong maximum at $2\theta\sim4.7°$, a new peak appears, the intensity of which increases at 130 K and thereafter seems to stabilize. At the same time, the intensity of the $2\theta=4.7°$ maximum decreases and at the lowest temperatures only a few spots remain visible on the Imaging-Plate image. At around $2\theta=12°$ and until a temperature of 150 K, two main lines are splitting, but below 140 K these lines fade out while a new one between them increases in intensity (see Figure 2, broken lines). At $2\theta\sim15°$ and below 170 K, some reflections seem to fade out and at 150 K a new peak appears in a position very close to that of the initial reflections, which becomes stronger as the temperature decreases.

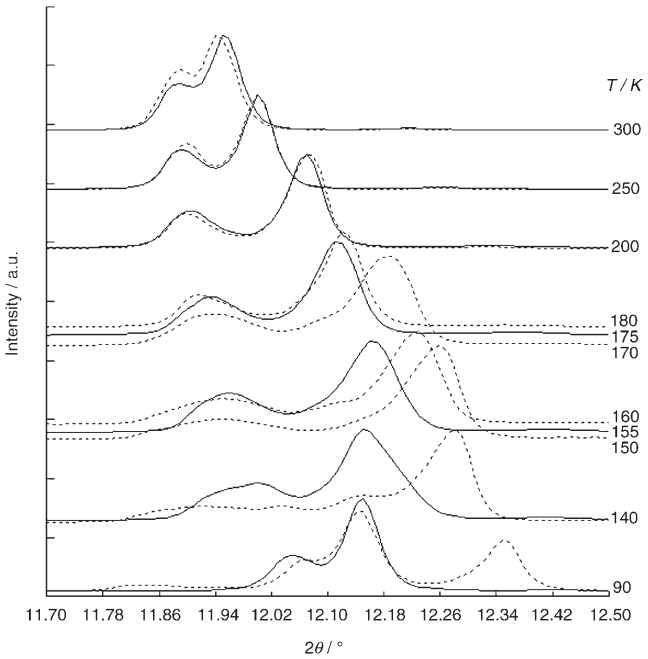

Figure 2. Excerpt of the diffraction patterns of the scan (-----) and long-term (——) experiments of $[Fe(teec)_6](ClO_4)_2$, showing their evolution as function of temperature.

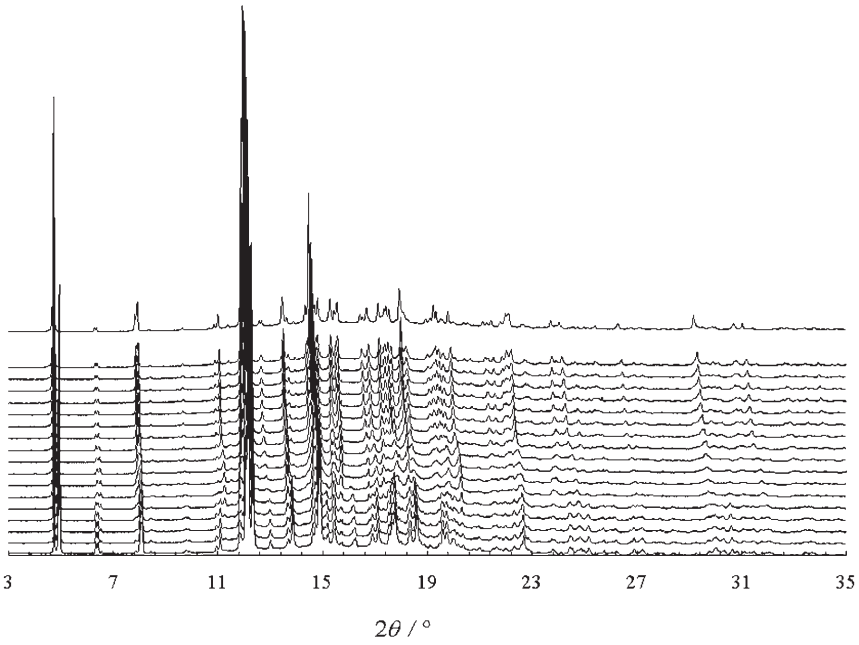

Figure 1. Diffraction patterns (3–35° 2θ) of the scan measurements of $[Fe(teec)_6](ClO_4)_2$, from top to bottom: 300 K and 250 K→90 K (in steps of 10 K).

Below 130 K the patterns seem to stabilize. It is remarkable that the temperature interval (180–130 K) in which these differences were observed coincides with the temperature interval for which the spin transition has been observed (Figure 3). A likely hypothesis is that, as the temperature decreases, the molecules cross over from the HS to the LS state in such a way that both spin states simultaneously give rise to observable and distinguishable diffraction patterns.

Inspection of the long-term and scan data at each temperature shows no significant differences in the interval 300–175 K. Below about 170 K till 130 K, however, the differences become prominent. The

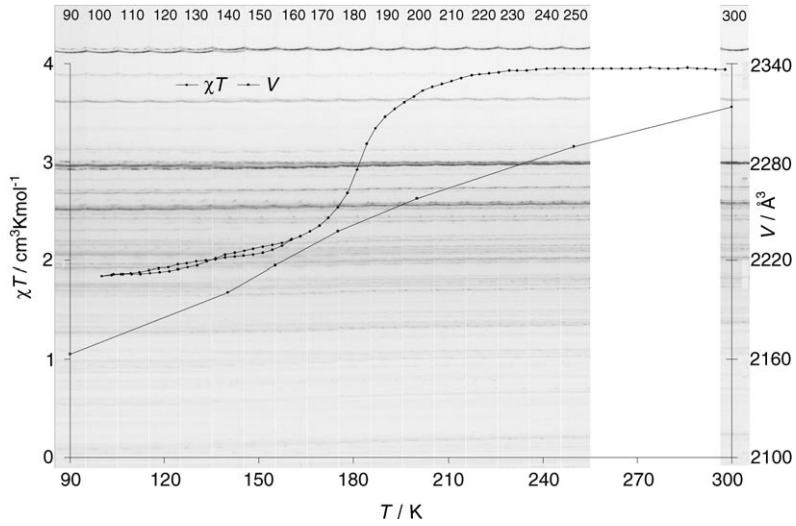

Figure 3. Magnetic susceptibility versus temperature, unit-cell volume as a function of temperature for long-term measurements of [Fe(teec)$_6$](ClO$_4$)$_2$ and Imaging-Plate data of the scan measurements (T↓ = 160–100 K and T↑ = 100–298 K).

long-term pattern at 175 K is still quite similar to the scan pattern at 180 K but differs appreciably from the scan pattern at 170 K especially in the interval $2\theta = 12$–$25°$ (Figure 1). Also the long-term data at 155 K differ considerably from the 150 and 160 K scan data in the interval $2\theta = 15$–$25°$. Comparing the scan and long-term patterns at 90 and also at 140 K, remarkable differences can be observed in the range $2\theta = 4$–$25°$.

Another observation is that the intensity peaks in several 2θ ranges are broader and less-well defined in the temperature intervals 140–170 K and 140–175 K for the scan and long-term data, respectively. This is likely to be caused by structural changes that take place during the data collection.

As explained above, in the scan data the diffraction patterns of both the HS and LS states occur simultaneously. For this reason, and because of the broadened and less well-defined peaks, a convincing unit-cell determination for the scan data was difficult to achieve. For the long-term data these problems were less serious, in spite of the presence of a small amount of the HS state phase evident in the LS long-term data. By using a laboratory-room-temperature Guinier powder diffraction pattern of [Fe(teec)$_6$](ClO$_4$)$_2$ as a reference, all long-term SPring8 (synchrotron located at the Japan Synchrotron Radiation Research Institute, Nishi-Harima, Hyogo, Japan) data could be indexed as monoclinic with $P2_1/c$ to be the most likely space group and $Z = 2$ in accordance with the density of the compounds [Fe(teeX)$_6$](BF$_4$)$_2$ (X = Cl, Br, I).[22–24] Table 1 lists unit-cell data while the unit-cell volume as a function of temperature is shown in Figure 3 together with the Imaging-Plate data of the scan measurements and the magnetic susceptibility versus temperature ($T\uparrow = 160$–100 K and $T\downarrow = 100$–298 K).

In Figure 4a the changes in the unit-cell axes and volume relative to their values at 90 K are plotted for the long-term data ($\Delta L = L_T - L_{90}$, $\Delta V = V_T - V_{90}$). Likewise, Figure 4b shows the behavior of the monoclinic angle β as function of temperature. In Figure 4c the percentage change of the unit-cell axes and volume relative to their values at 300 K is depicted: $[(L_T - L_{300})/L_{300}] \cdot 100\,\%$, with L_T being a unit-cell axis or volume value at temperature T. The final contraction percentages at 90 K show a relatively large contraction of the a axis (4.5 %) compared to those for the b axis (1.1 %) and c axis (1.0 %). Results of the full-pattern decomposition and Pawley refinement using the Material Studio (MS) package[25] are summarized in Table 2.

Table 1. Unit-cell parameters for long-term data of [Fe(teec)$_6$](ClO$_4$)$_2$ (refinement with Materials Studio software) as a function of temperature.

T[K]	a[Å]	b[Å]	c[Å]	β[°]	V[Å^3]
90	11.6214(2)	17.7883(3)	10.46283(19)	90.3470(16)	2162.89(8)
140	11.8900(4)	17.7246(4)	10.4418(3)	90.348(2)	2200.52(12)
155	11.9962(4)	17.6797(4)	10.4528(3)	90.279(4)	2216.90(15)
175	12.02833(17)	17.7513(2)	10.47896(18)	90.232(2)	2237.43(7)
200	12.0833(3)	17.8039(3)	10.4934(2)	90.196(2)	2257.43(9)
250	12.14157(18)	17.8964(2)	10.53631(15)	90.3846(12)	2289.39(6)
300	12.1669(3)	17.9845(3)	10.5736(2)	90.6044(13)	2313.54(9)
Guinier data	12.232(5)	18.055(6)	10.627(3)	90.59(2)	2347(1)

Structure determination from synchrotron powder data: In the structure determination process by using the 300 K data, two models were found, referred to as M1 and M2. Both models are similar to the room-temperature structure of [Fe(teec)$_6$](BF$_4$)$_2$,[22] except for an anti-parallel orientation of the tetrazole ring of ligand a in M1. Although after the final Rietveld refinement (RR) with GSAS[26] both models did not differ much in terms of criteria-of-fit (see Table 3) and difference pattern (Figure 5), model M2 was considered to be slightly better and assumed to be the most likely structural model of [Fe(teec)$_6$](ClO$_4$)$_2$ at 300 K, also because its packing is similar to that of [Fe(teec)$_6$](BF$_4$)$_2$. The refinement results of M1 and M2 indicate that RR and the R_{wp} are not very sensitive to differentiate between small structural differences, like those present between M1 and M2, especially when the experimental data are not ideal. The problems with the sample granularity, assumed to be responsible for the lower data quality, were less severe in the long-term data due to spinning the capillary, but could not be eliminated completely. A more extensive grinding of the compound could not be applied as it led to a significantly different diffraction pattern.

The structure at 90 K was refined successfully (Figure 6) starting from the structural model at 300 K, though not

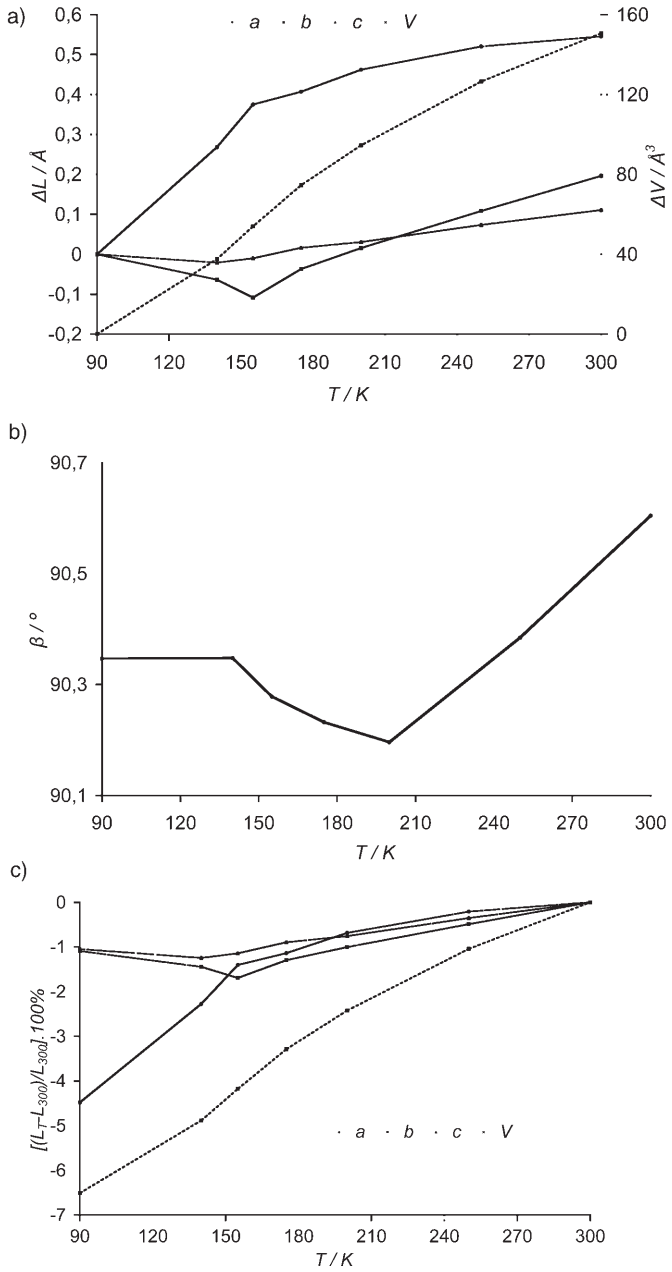

Figure 4. a) Changes in the unit-cell axes and volume relative to their values at 90 K, as a function of temperature T for long-term measurements of $[Fe(teec)_6](ClO_4)_2$. b) The angle β as function of temperature T. c) Change of the unit-cell axes and volume relative to their values at 300 K [%].

Table 3. Summary of the Rietveld refinement results of the $[Fe(teec)_6](ClO_4)_2$ models.

T[K]	300 (MS)	300 (GSAS-M1)	300 (GSAS-M2)	155 (MS)	90 (GSAS)
R_p[%][a]	5.09	3.29	3.28	5.45	3.52
R_{wp}[%]	8.08	4.58	4.58	7.75	4.70
2θ range[°]	3–50	2.5–50	2.5–50	3–51	2.5–66
resolution[Å]	1.18	1.18	1.18	1.16	0.92

[a] $R_{wp} = \left[\frac{\sum w_i(y_{oi}-y_{ic})2}{\sum w_{iy_{oi}}^2}\right]^{1/2}$; y_{oi} = observed intensity at the i^{th} datapoint, y_{ci} = calculated intensity at the i^{th} datapoint, $w_i = 1/y_{oi}$, subscript i denotes all points in the pattern range undergoing refinement.

without difficulty because of ice formation and the presence of a (small) quantity of the HS state phase. The presence of this HS phase affected the diffraction patterns when digitized from the Imaging-Plate images: a slightly different choice of integration area led to different integrated intensities as shown in Figure 7.

Structure of $[Fe(chloroethyltetrazole)_6](ClO_4)_2$: In all Rietveld refinements of $[Fe(teec)_6](ClO_4)_2$, restraints were essential to avoid distortion of the structural model. Therefore, values of bond lengths and angles should be considered to be indicative and not absolute. Like in the other $[Fe(teeX)_6](BF_4)_2$ (X = Cl, Br, I) complexes,[22–24] the Fe atom in the centrosymmetric $[Fe(teec)_6]^{2+}$ moiety is at a special position and is octahedrally coordinated by the neighboring nitrogen atoms at distances 2.174(9)–2.188(9) Å at 300 K that are typical Fe–N distances in the HS state. The Fe–N distances in the structure at 90 K are 1.909(7)–2.091(8) Å, which corresponds to an average Fe–N bond length decrease of 7.8% (0.17 Å).

All N-Fe-N angles show almost ideal octahedral symmetry with a maximum deviation of 1.5(3)° from 90° at 300 K and 2.9(3)° at 90 K. At 300 K, the four in-plane N atoms form an almost perfect square (deviation smaller than 0.5° from 90°). At 90 K, the square is distorted with a maximum deviation of 5.2° from 90°. Distances and angles given in the text containing estimated standard deviations (esds) have been calculated with the program PLATON;[27] those not containing esds have been calculated with DIAMOND[28] or PLUVA.[29]

In Figure 8a the refined structures at 300 and 90 K have been superimposed. All figures displaying the structure have been generated with the programs DIAMOND and PLUVA, while in Figure 8b, the molecular structure with

Table 2. Full-pattern decomposition (MRIA) and Pawley refinement (Materials Studio software) results for long-term measurements of $[Fe(teec)_6](ClO_4)_2$.

T[K]	300 (MRIA)	300 (MS)	250 (MS)	200 (MS)	175 (MS)	155 (MS)	140 (MS)	90 (MRIA)	90 (MS)
R_p[%]	2.54	1.98	1.83	1.95	1.68	2.26	1.91	3.66	1.97
R_{wp}	4.12	2.77	2.90	3.41	2.87	3.75	3.42	5.97	3.27
2θ range[°]	2–28.65	3–25	3–35	3–35	3–35	3–25	3–35	2–29.61	3–35
resolution[Å]	2.02	2.31	1.66	1.66	1.66	2.31	1.66	1.96	1.66
excluded regions[°]						15.60–15.75 16.65–16.75 17.30–17.42			

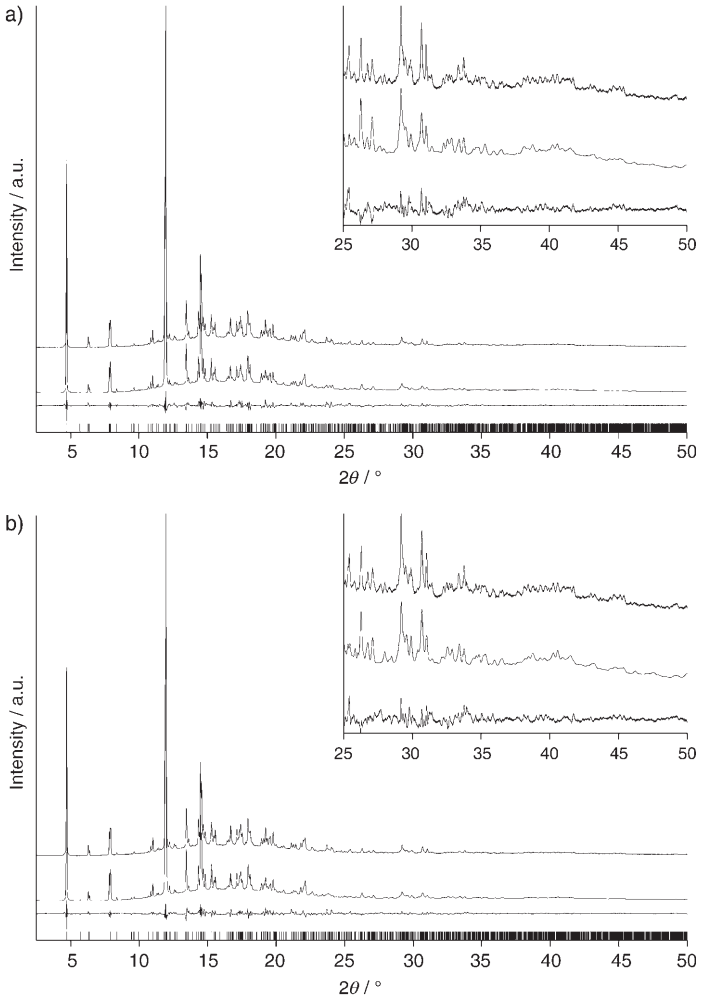

Figure 5. Rietveld refinement (GSAS) plots for [Fe(teec)$_6$](ClO$_4$)$_2$ at 300 K for: a) Model M1 and, b) Model M2 experimental diffraction pattern (upper); the pattern as calculated from the refined crystal structure (middle); difference between these patterns (lower), and; reflection positions (vertical lines).

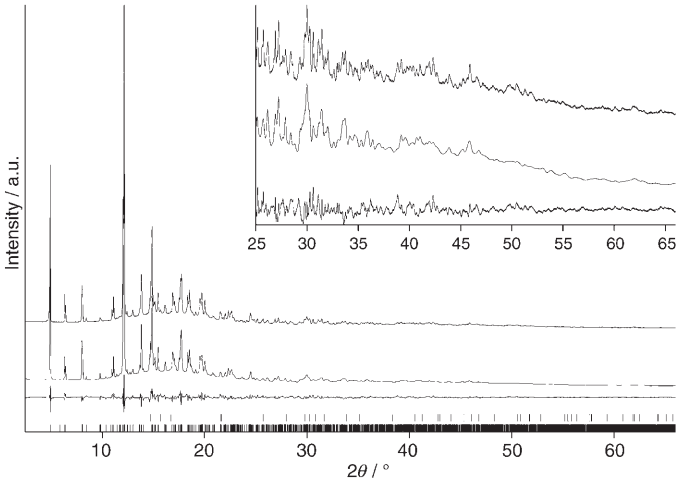

Figure 6. Rietveld refinement (GSAS) plot for [Fe(teec)$_6$](ClO$_4$)$_2$ at 90 K: Experimental diffraction pattern (upper); the pattern as calculated from the refined crystal structure (middle); the difference between these patterns (lower); ice peaks (upper row of vertical lines) and; reflection positions (lower row of vertical lines).

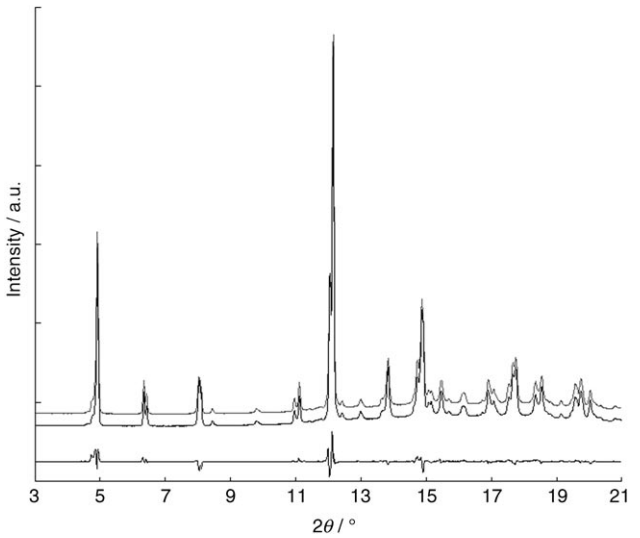

Figure 7. Excerpt of two diffraction patterns of the [Fe(teec)$_6$](ClO$_4$)$_2$ at 90 K, as integrated from the Imaging Plate by using two different integration areas. The lowest line is the difference between them.

the numbering of the non-hydrogen atoms in the asymmetric unit is shown. From the superposition of the structures it is concluded that the major changes are limited to the position and orientation of the ethyl groups, those of ligand c having changed the most and those of ligand b the least. In contrast, the tetrazole rings hardly changed, being almost parallel at the two temperatures.

The structure of [Fe(teec)$_6$](ClO$_4$)$_2$ is layered along the unit-cell axes, like in [Fe(teeX)$_6$](BF$_4$)$_2$ (X = Cl, Br, I). In Figure 9 the layers parallel to the *b* and *c* axes and almost perpendicular to the *a* axis are shown while in Figure 10 they are viewed along the *a* axis. The differences between the structures at the two temperatures mainly concern the orientation of the Cl–C bonds in ligand c that are almost parallel to the *b* and *c* axes at 300 K (within 15° deviation) while at 90 K, this deviation is 35°. The distance between the structural layers is around 2.3 Å at 300 K and 1.8 Å at 90 K (it is noted that the reported interlayer distances have been estimated visually, the layers being viewed along the *b* and *c* axes; therefore they are given as indicative and mostly for comparative reasons). Interlayer-short-contacts interactions exist between Cl and hydrogen atoms (Table 5) and this interaction seems to be stronger at 90 K, a similar observation as for the tetrafluoroborate complex.[24] In Table 6 possible intermolecular hydrogen bonds are listed. According to PLATON, three Cl···H–C bonds at 300 K are short enough to be considered as hydrogen bonds, one of them being an intralayer hydrogen bond (Cl1···H3a2–C3a) and almost parallel to the *c* axis, and the other two being interlayer hydrogen bonds. At 90 K the Cl···H–C hydrogen bond network appears stronger. The N···H–C bonds (Table 6) are rather long compared to those in the tetrafluoroborate com-

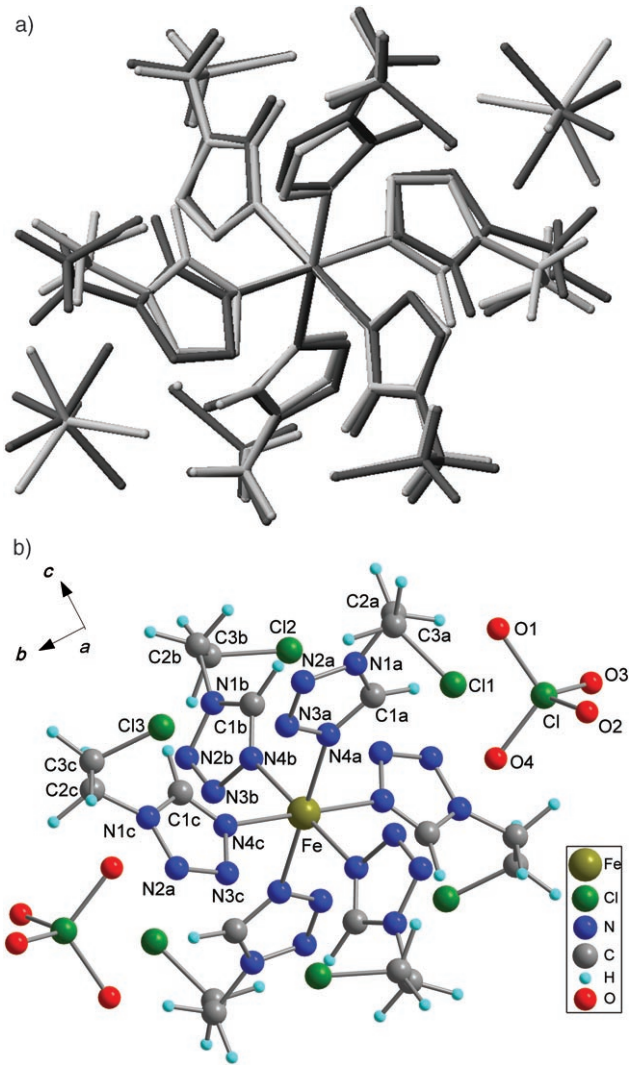

Figure 8. a) The refined structures at 300 (dark gray) and 90 K (light gray) superimposed; b) molecular crystal structure of $[Fe(teec)_6](ClO_4)_2$ at 300 K showing the numbering scheme.

Table 4. Restraints terms in the least-squares minimization function of the Rietveld refinement of $[Fe(teec)_6](ClO_4)_2$ (GSAS). At 300 K: $f_d = 3$, $f_a = 10$, and $f_p = 15$. At 90 K: $f_d = 12$, $f_a = 20$, and $f_p = 20$.

T[K]	300 (M1)	300 (M2)	90
bond lengths (46)	5565.5	4115.4	4010.7
bond angles (78)	5879.6	6370.2	8396.7
planar group (15)	2952.8	3083.9	2880.5
total data (300 K:4888; 90 K:6462) (powder+restraints)	69912	68983	114400

Table 5. Interlayer shorts contacts in $[Fe(teec)_6](ClO_4)_2$ at 300 and 90 K (the second line denotes the number of contacts in each case).

T[K]	Cl–Cl < 4.4 Å	Cl–H < 3.5 Å	H–H < 3.5 Å
300	4.091–4.226	2.70–3.49	2.03–3.38
	3 (1 intralayer)	5	5
90	3.916–4.176	2.34–3.50	2.21–3.31
	3 (1 intralayer)	6	5

Table 6. Possible intermolecular hydrogen bonds (lengths [Å], angles [°]) of $[Fe(teec)_6](ClO_4)_2$ at 300 K and 90 K.

	300 K			90 K		
N···H	N···C	N-H-C	N···H	N···C	N-H-C	
N2a···H2b2−C2b	2.84	3.70	134	3.16	3.99	133
N2b···H2a1−C2a	2.74	3.50	126	2.67	3.40	124
N2c···H2c1−C2c	2.82	3.59	127	3.61	3.63	83
	Cl···H	Cl···C	Cl-H-C	Cl···H	Cl···C	Cl-H-C
Cl1···H3a2−C3a	2.81(4)	3.68(2)	137(3)	2.68(3)	3.65(2)	150(2)
Cl3···H3b1−C3b	2.70(5)	3.53(2)	130(3)	2.34(4)	3.266(19)	139(3)
Cl2···H3b2−C3b	2.82(4)	3.83(2)	154(3)	2.95	3.90	149

plex.[24] From the N···H distances it can be concluded that, just as in the case of the tetrafluoroborate complex, at 300 K more N···H−C hydrogen-bond stabilization exists than at 90 K. Actually, at 90 K two of the three N···H distances are too long to be considered as hydrogen bonds.

Discussion

Spin-crossover behavior: To explain the spin-crossover phenomenon two main types of thermodynamic models have been proposed, one being based on the hypothesis of regular solutions and the other on the idea of spin-domain formation within the crystal lattice. According to the regular-solution model[30–32] the origin of the intermolecular interactions lies in the elasticity of the medium. A volume change of a few molecules uniformly distributed over the crystal, by replacing atoms of different size or by the spin-state change of spin-crossover molecules, may give rise to lattice strain and this, in turn, to long-range interactions that may be interpreted as an internal pressure that increases linearly with the concentration of the LS species and affects all molecules in the crystal by the same strength (independently of distances).

In the theoretical model proposed by Sorai and Seki,[33] and explored further by Bolvin and Kahn,[34] it is assumed that the molecules cluster in domains with identical spin (HS or LS domains) as a result of high cooperativity and that the conversion of the electronic state occurs simultaneously in a group of molecules that form a "cooperative" region.

As it turns out, unlike the cases of $[Fe(teeX)_6](BF_4)_2$ (X = Cl, Br, I),[23,24,35] in $[Fe(teec)_6](ClO_4)_2$ a nongradual evolution of the diffraction patterns as a function of temperature is observed and two similar but distinguishable lattices occur, the quantities of which vary with the temperature, a behavior suggesting an isostructural phase transition. The lattice observed at 300 K is attributed to the HS state, and the one appearing below 170 K to the LS state. The scan SRPD experiments revealed the simultaneous presence of HS and LS domains that are large enough to give their own distinctive diffraction patterns, a phenomenon that was not observed in the cases of $[Fe(teeX)_6](BF_4)_2$ (X = Cl, Br, I). This observation supports the theory that domains with the same spin can be formed during spin crossover.

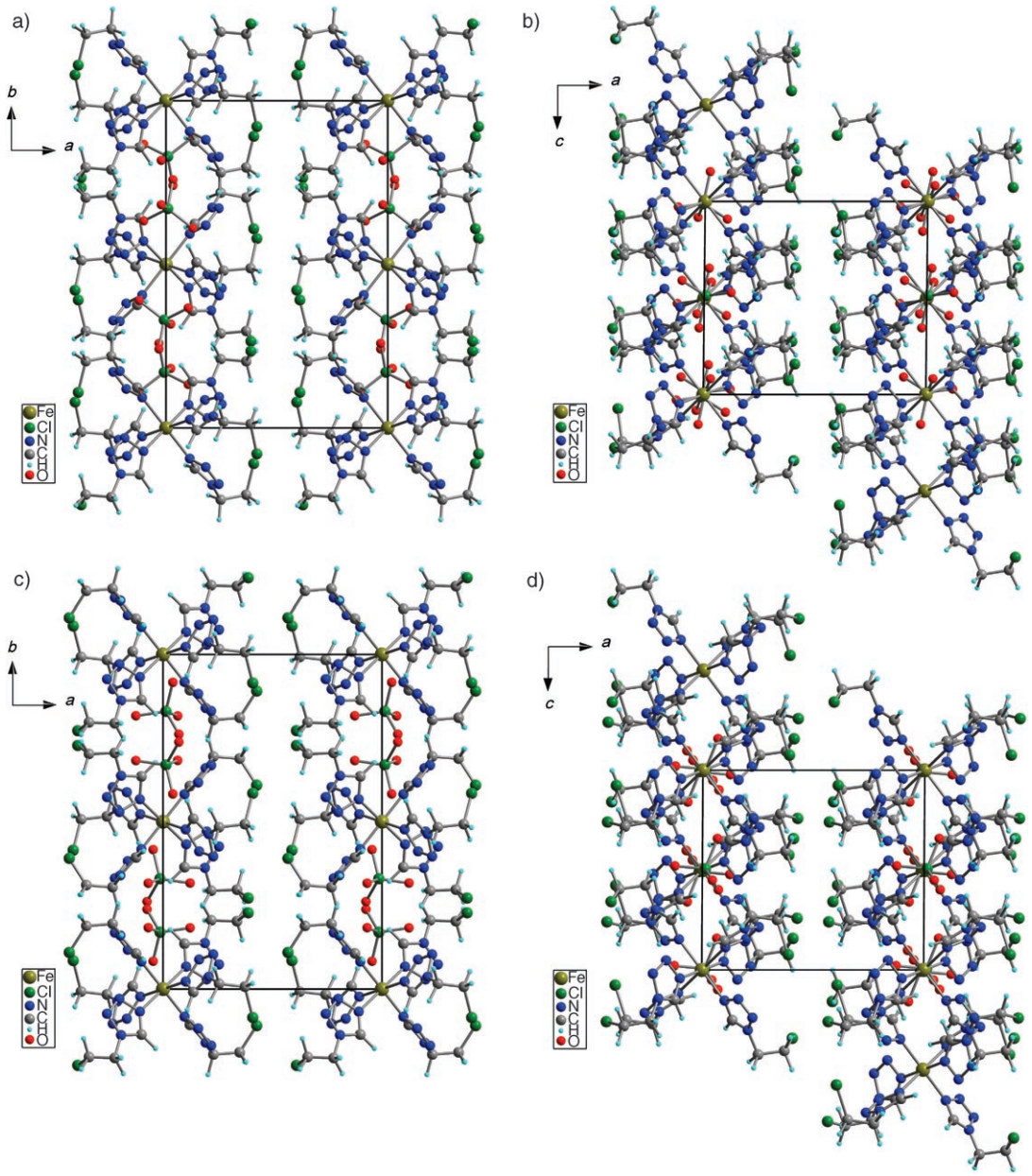

Figure 9. The [Fe(teec)$_6$](ClO$_4$)$_2$ structure at: a),b) 300 K and; c),d) 90 K form layers along the *b* and *c* axes (a),c) and b),d), respectively) perpendicular to the *a* axis.

Spin-like domain formation has been reported recently[36] for the compound [Fe(btr)$_2$(NCS)$_2$](H$_2$O), which exhibits a complete and abrupt spin transition at 123.5 K in cooling mode and shows a hysteresis of 21 K. Time-resolved single-crystal diffraction experiments (150 s duration each) carried out at the temperature of spin transition revealed the continuous and complete conversion of the HS state to the LS state through an intermediate situation for which both spin states coexist.

Anisotropy of unit-cell contraction and long-term versus scan data: As in the case of the long-term experiments of [Fe(teec)$_6$](BF$_4$)$_2$,[24] the final lattice contractions of [Fe(teec)$_6$](ClO$_4$)$_2$ relative to the values at 300 K show a remarkable anisotropy along the *a* axis, although the anisotropy in the latter compound is somewhat larger. In both complexes, the *c* axis contracts the least. The changes in unit-cell parameters are not linear and although all axes change rather gradually, after the completion of the largest part of the spin crossover (~155 K) the *a* axis contracts faster while the *b* and *c* axes increase slightly. In the case of [Fe(teec)$_6$](BF$_4$)$_2$ the most significant deviations from the long-term unit-cell changes in the lattice parameters were observed practically after the completion of the first SCO. Although unit cells from the scan measurements have not been determined for the [Fe(teec)$_6$](ClO$_4$)$_2$ and therefore no conclu-

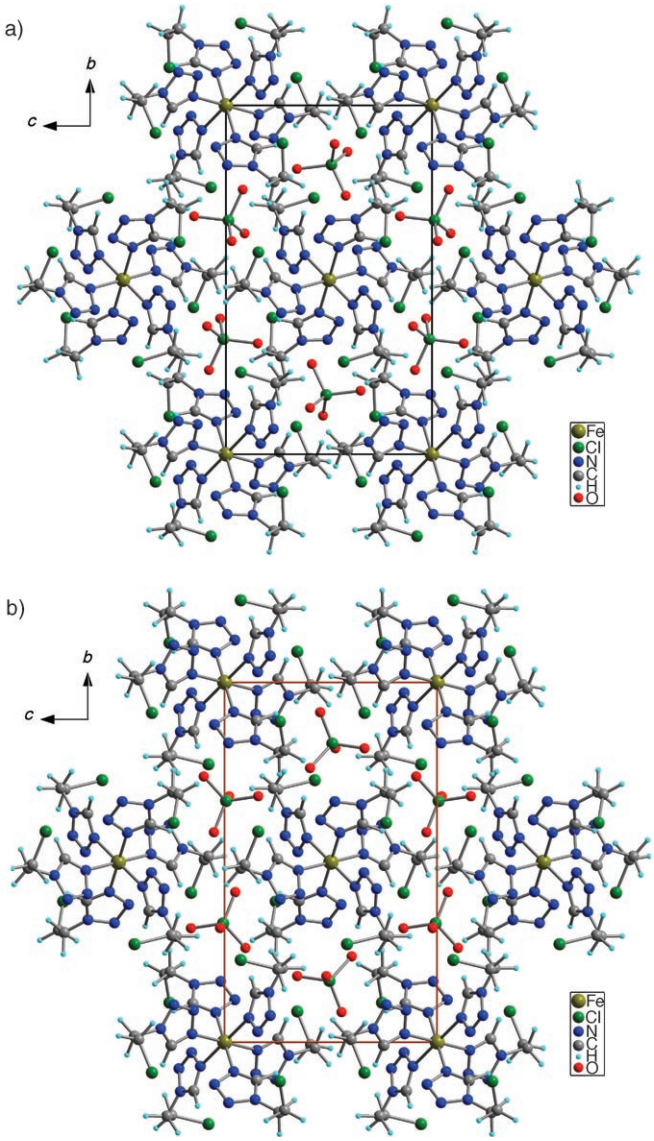

Figure 10. View of the $[Fe(teec)_6](ClO_4)_2$ structure at 300 K (a) and 90 K (b) along the *a* axis; within these layers the Fe and B atoms exhibit a pseudotrigonal symmetry.

sion can be drawn about the anisotropy in the contraction direction, the reasoning about the direction of the anisotropy may apply here as well: After the SCO takes place, the modified lattice vibrations (mainly due to the Fe–N bond-length shrinkage) are transmitted to the rest of the molecule. The first way for the vibrations to be transmitted is within the *bc* planes as the intralayer–intermolecular contacts and interactions (hydrogen bonds) are stronger than the interlayer contacts. After the intralayer relaxation, the contractions occur in directions where more space is available, that is, along the *a* axis. If this hypothesis is correct, the long-term data of $[Fe(teec)_6](ClO_4)_2$ reflect only the later structural changes. However, in the case of $[Fe(teec)_6](BF_4)_2$ there was no indication of the existence of two separate diffraction patterns while in the case of $[Fe(teec)_6](ClO_4)_2$ there is clear evidence.

As described above, noticeable differences exist between the scan and long-term data collected at the same temperature. These differences can be attributed to the relaxation of the structure during the long-term measurements, a conclusion drawn also in the case of $[Fe(teec)_6](BF_4)_2$.[24] Indeed, inspection of the long-term diffraction patterns at 155–90 K does not show a significant amount of HS state.

Structural aspects: In $[Fe(teec)_6](ClO_4)_2$ the Fe^{II} atoms are on only one type of crystallographic site, like in $[Fe(teeX)_6](BF_4)_2$ (X = Cl, I, Br),[23,24] therefore the incomplete SCO cannot be attributed to the existence of two Fe^{II} ions behaving differently, one of which does not undergo SCO, as in the case of $[Fe(mtz)_6]X_2$, X = BF_4^-, ClO_4^-.[18,19] A comparison of $[Fe(teec)_6](ClO_4)_2$ with other Fe–N bonds of SCO compounds, in particular those that also exhibit an incomplete SCO, reveals no clear common structural characteristics, except for a decrease of the Fe–N bond length. The average decrease of the Fe–N bond length (0.17 Å) in $[Fe(teec)_6](ClO_4)_2$ is clearly smaller than in $[Fe(teec)_6](BF_4)_2$ (0.31 Å, two-step complete SCO) and this may be related to the incomplete HS→LS spin transition as observed by using magnetic susceptibility measurements (Figure 3).

A similar Fe–N contraction (0.15 Å) has been observed in $[Fe(PM\text{-}TeA)_2(NCS)_2]\cdot CH_3OH$ (PM = *N*-2′-pyridylmethylene, TeA = 4-aminoterphenyl),[11] that also exhibits a smooth and incomplete spin crossover. This molecule is also centrosymmetric with the octahedrally coordinated Fe^{II} atom at a special position. For this compound it was concluded, on the basis of single-crystal structures determined at 298 K, 140 K, and 11 K (all space groups *Pccn*), that no structural phase transition was involved in the HS→LS SCO.

In the case of $Fe(btz)_2(NCS)_2$ (btz = 2,2′-bi-4,5-dihydrothiazine),[37] which also shows a gradual incomplete spin crossover, the determined single-crystal X-ray diffraction structures at room temperature and 130 K (space group *Pbcn*, *Z* = 4) showed no evidence of structural phase transition. The general conformation of the complex was nearly unchanged upon cooling and the most significant variations concerned the $Fe–N_6$ core (average Fe–N bond contraction of 0.17 Å).

Conclusion

Although the above suggests that an incomplete HS→LS spin crossover can be characterized by a Fe–N bond-length decrease, it should be taken into account that the structures reported both here and in the literature are based on long-term data. The scan data point out that during a short period of time $[Fe(teec)_6](ClO_4)_2$ behaves as two phases with distinct diffraction patterns, the ratios of which change as the temperature changes along the spin-crossover trajectory. These structures are likely to be related to the two magnetic phases (HS and LS) but not necessarily the same as the structures that result after a longer relaxation. Con-

sidering the remarkable differences between the scan and long-term measurements due to the significant structure relaxation occurring in the latter, one cannot safely draw conclusions about the precise mechanism of the incomplete spin crossover on the basis of long-term structures alone. A similar conclusion was drawn in the case of [Fe(teec)$_6$](BF$_4$)$_2$.[24]

Most attempts so far to interpret the spin-crossover mechanism have been based on structural data obtained from long-term experimental data. The experimental work described in this article and in references [23,24], and [35] points out that important structural information may be missed when only long-term experiments are conducted and suggests that experiments with SCO complexes on a much shorter time scale should be carried out as well. It has become clear that the duration of experiments is an important experimental parameter. Suitable experimental set-ups, as for example that of the BL02B2 beam line at SPring8, can greatly facilitate the execution of these types of experiments.

Experimental Section

X-ray powder data collection: [Fe(teec)$_6$](ClO$_4$)$_2$ (white crystallites) was synthesized as described in [20] and [21]. The first data set of a sample (batch 1) was collected using a Guinier–Johansson camera at room temperature from which the unit cell could be determined, though with difficulty because of the amount of impurity (~3%) present. The impurity percentage agreed with that suggested from the lower-temperature ^{57}Fe Mössbauer experiments. Owing to the impurity level, no attempts were made to determine the crystal structure from these data. Instead, a new batch 2 was synthesized in the same way as batch 1 and this batch turned out to contain no significant amount of impurity.

The temperature-dependent data set series of batch 2 (called from now on SPring8 data) were collected by using a large Debye–Scherrer camera (radius 286.5 mm) and an Imaging-Plate detector[38] installed at the BL02B2 beamline of SPring8 (Japan Synchrotron Radiation Research Institute, Nishi-Harima, Hyogo, Japan), by using a 0.4 mm capillary and $\lambda =$ 0.999995 Å. Details of the experimental set-up at SPring8 are provided elsewhere.[24,35]

Short exposures (5 min) of several samples of batch **2** were carried out at 300 K to check the quality of the powder samples. Almost all diffraction patterns were granular, likely to have been caused by insufficient particle statistics (large crystallites). However, a more intensive powdering of the samples led to a completely different type of diffraction pattern (data not shown), possibly due to a phase transition induced by pressure, and therefore a compromise had to be made and the sample with the least granular pattern was selected for the longer experiments.

Subsequently, at a series of temperatures (300 K, and from 250 to 90 K in steps of 10 K), data collection was carried out for 5 min at each temperature. To avoid temperature overshoot, a temperature-stabilization period was applied before starting each data collection. The temperature-stabilization time from 300 to 250 K was 240 s and for all lower temperatures 160 s. In total 18 diffraction patterns were collected within almost 137 min.

After inspection of the diffraction patterns, several temperatures were selected for the long-term measurements (50 min): 300, 250, 200, 175, 155, 140, and 90 K, by using a temperature-stabilization time of 5 min each, which led to a 6 h 20 min total-data-collection time. From the temperature difference over the sum of the temperature-stabilization period and data collection time, the average temperature drop ΔT (K min^{-1}) for each experiment could be calculated (Table 7). After the long-term experiments, the color of the compound was light orange.

Table 7. Average temperature drop ΔT [K min^{-1}] in [Fe(teec)$_6$](ClO$_4$)$_2$ experiments.

Scan measurements (5 min)		Long-term measurements (50 min)	
step	ΔT	step	ΔT
300→250	5.55	300→250, 250→200, 140→90	0.91
rest	1.3	200→175	0.45
		175→155	0.36
		155→140	0.27

Structure solution and refinement: The powder diffraction patterns were indexed by using either the program ITO[39] or the local program LSQDETC.[40] The unit cells of the SPring8 long-term experiments were refined by using the Tomandl–Pseudo-Voigt profile function for the Pawley refinement as incorporated in the Materials Studio (MS) package.[25] The SPring8 diffraction patterns at 300 and 90 K were also decomposed into X_{obs} values with the full-pattern decomposition module of the program MRIA[41] by using a split-type Pseudo-Voigt profile function.[42]

The structures have been solved with direct-space methods and the required initial search model was constructed from the structure of [Fe(teec)$_6$](BF$_4$)$_2$ at room temperature[22] with [BF$_4$]$^-$ being replaced by [ClO$_4$]$^-$ by using the Materials Studio package. As in the case of [Fe(teec)$_6$](BF$_4$)$_2$, the molecule is centrosymmetric with Fe at a special position and only half of it was required as a search model (consisting of the (teec)$_3$ moiety and the ClO$_4^-$ ion). In the searches 18 degrees of freedom (DOF) were used, consisting of three rotational parameters and nine torsion angles for the (teec)$_3$ moiety and six parameters (three translational and three rotational) for the ClO$_4^-$ ion (for the definition of DOF see reference [22] and/or reference [24]).

Two direct-space methods were used to solve the structure at 300 K, the parallel tempering (PT) procedure in Powder Solve[43] of the Materials Studio package and a genetic algorithm (GA) that has been implemented in the program suite MRIA. In the GA implementation, developed at the Laboratory of Crystallography (University of Amsterdam),[44] a "parameter box" is created around the solution of a cycle (typical sizes are 1.5 Å, 10°, and 30° for translational, rotational, and torsion parameters, respectively). The box size is varied dynamically, thus allowing smaller or larger area searches. In this GA five boxes can be searched in parallel, in addition to the search in the user-defined parameter space. More details on the GA and its results can be found in reference [35].

In the structure determination process by using the data obtained at 300 K, with both PT and GA, two models were found, referred to as M1 and M2. Both models are similar to the room-temperature structure of [Fe(teec)$_6$](BF$_4$)$_2$,[22] except for an antiparallel orientation of the tetrazole ring of ligand a in M1.

With PT and by using data in the range $2\theta = 3$–25° (resolution $d =$ 2.31 Å), models of type M1 were found ($R_{wp} = 11.39\%$) and processed further with the RR module of the Materials Studio package.[25] The GA method, by using the (with the Materials Studio software) refined structure M1 as initial model, delivered both M1 and M2 models, depending on the precise settings of the parameters. The run that led to the M1 model ($R(X) = 0.50$) was carried out with 100 X_{obs} values ($2\theta_{max} = 21.98$°, $d_{min} = 2.62$ Å) while the run that led to the M2 model ($R(X) = 0.522$) was carried out with 120 X_{obs} values ($2\theta_{max} = 23.45$°, $d_{min} = 2.46$ Å).

Rietveld Refinement of the M1 model obtained with the PT method was initially carried out with the MS program package. The Fe(teec)$_6$ moiety and the ClO$_4^-$ ion were refined as rigid bodies and the torsion angles were refined as well. Attempts to relax the model and to refine individual atomic coordinates resulted only in an unacceptable distortion of the model. Therefore, the RR was completed with the program GSAS[26] by using the interface EXPGUI[45] because of the more-sophisticated handling of geometrical restraints (bond distance, bond angle, and planar). The same program was used for the RR of the M2 model obtained with the GA method. A special type of Pseudo-Voigt function (profile function type 3 in GSAS) was used to model reflection asymmetry. Texture was corrected for by using up to sixth-order spherical harmonic functions.

Zero-point correction and cell-parameter refinement were applied as well.

After the refinement both models did not differ much in terms of criteria-of-fit (see Table 3) and difference pattern (Figure 5). Model M2 is considered to be slightly better and, because its packing is similar to that of $[Fe(teec)_6](BF_4)_2$, is assumed to be the most likely structural model of $[Fe(teec)_6](ClO_4)_2$ at 300 K.

For the structure at 90 K an almost refined structural model M2 of $[Fe(teec)_6](ClO_4)_2$ at 300 K was used as the starting point of the refinement with GSAS. The hexagonal ($P6_3/mmc$) phase of ice[46] with $a=b=4.523$, $c=7.367$ Å was introduced as a second phase into the RR because of ice formation outside the capillary. After fitting the ice phase by using the same profile function as for the main phase, all its parameters were kept constant and only those of the $[Fe(teec)_6](ClO_4)_2$ phase were being refined. The final plot of the observed, calculated, and difference patterns after RR at 90 K is shown in Figure 6.

Both at 300 and 90 K, bond-length, bond-angle, and planarity restraints were applied. The final values of the global weighting factors and the contribution of every group of restraints to the final χ^2 are shown in Table 4. Atomic displacement parameters of the non-hydrogen atoms were refined isotropically and they were constrained such that all atomic displacement parameters of each type of element were the same (in addition, $U_C=U_N$ except for the C atoms connected to Cl atoms).

Spherical-harmonics coefficients up to sixth-order were refined and the final texture index was $J=2.264$ for model M1, $J=2.598$ for model M2 at 300 K, and $J=2.163$ at 90 K, suggesting a considerable preferred orientation.

CCDC-274916 and CCDC-274917 contain the supplementary crystallographic data for this paper. These data can be obtained free of charge from the Cambridge Crystallographic Data Centre via www.ccdc.cam.ac.uk/data_request/cif.

Acknowledgements

The authors thank Prof. Dr. M. Takata and Dr. E. Nishibori for their help during the powder diffraction experiments at SPring8 (JASRI, Japan). Dr A. F. Stassen is thanked for providing the investigated compound. E. J. Sonneveld is thanked for recording and indexing the Guinier diffraction pattern. E.D. acknowledges Accelrys Inc. for allowing the use of the Materials Studio software for evaluation purposes.

[1] P. Gütlich, A. Hauser, H. Spiering, *Angew. Chem.* **1994**, *106*, 2109–2141; *Angew. Chem. Int. Ed. Engl.* **1994**, *33*, 2024–2054.
[2] P. Gütlich, A. Hauser, *Coord. Chem. Rev.* **1990**, *97*, 1–22.
[3] Spin Crossover in Transition Metal Complexes I in *Topics in Current Chemistry, Vol. 233* (Eds.: P. Gütlich, H. A. Goodwin), Springer, Berlin, Germany, **2004**.
[4] O. Kahn, J. Kröber, C. Jay, *Adv. Mater.* **1992**, *4*, 718–728.
[5] C. Jay, F. Grolière, O. Kahn, J. Kröber, *Mol. Cryst. Liq. Cryst. Sci. Technol. Sect. A* **1993**, *234*, 255–262.
[6] J. Kröber, E. Codjovi, O. Kahn, F. Grolière, C. Jay, *J. Am. Chem. Soc.* **1993**, *115*, 9810–9811.
[7] O. Kahn, C. Jay Martinez, *Science* **1998**, *279*, 44–48.
[8] P. Gütlich, Y. Garcia, H. A. Godwin, *Chem. Soc. Rev.* **2000**, *6*, 419–427.
[9] J.-F. Létard, P. Guionneau, L. Goux-Capes, *Top. Curr. Chem.* **2004**, *235*, 221–249.
[10] A. F. Stassen, M. Grunert, E. Dova, H. Schenk, G. Wiesinger, W. Linert, J. G. Haasnoot, J. Reedijk, *Eur. J. Inorg. Chem.* **2003**, 2273–2282.
[11] P. Guionneau, J.-F. Létard, D. S. Yufit, D. Chasseau, G. Bravic, A. E. Goeta, J. A. K. Howard, O. Kahn, *J. Mater. Chem.* **1999**, *9*, 985–994.
[12] J.-A. Real, I. Castro, A. Bousseksou, M. Verdaguer, R. Burriel, J. Linares, F. Varret, *Inorg. Chem.* **1997**, *36*, 455–464.
[13] Y. Garcia, O. Kahn, L. Rabardel, B. Chansou, L. Salmon, J. P. Tuchagues, *Inorg. Chem.* **1999**, *38*, 4663–4670.
[14] J. G. Haasnoot, *Coord. Chem. Rev.* **2000**, *200*, 131–185.
[15] Spin Crossover in Transition Metal Complexes III in *Topics in Current Chemistry, Vol. 235* (Eds.: P. Gütlich, H. A. Goodwin), Springer, Berlin, Germany, **2004**.
[16] P. L. Franke, PhD Thesis, Leiden (The Netherlands), **1982**.
[17] P. L. Franke, J. G. Haasnoot, A. P. Zuur, *Inorg. Chim. Acta* **1982**, *59*, 5–9.
[18] L. Wiehl, *Acta Crystallogr. Sect. B* **1993**, *49*, 289–303.
[19] R. Hinek, H. Spiering, D. Schollmeyer, P. Gütlich, A. Hauser, *Chem. Eur. J.* **1996**, *2*, 1427–1434.
[20] A. F. Stassen, E. Dova, J. Ensling, H. Schenk, P. Gütlich, J. G. Haasnoot, J. Reedijk, *Inorg. Chim. Acta* **2002**, *335*, 61–68.
[21] A. F. Stassen, PhD Thesis, Leiden (The Netherlands), **2002**.
[22] E. Dova, A. F. Stassen, R. A. J. Driessen, E. Sonneveld, K. Goubitz, R. Peschar, J. G. Haasnoot, J. Reedijk, H. Schenk, *Acta Crystallogr. Sect. B* **2001**, *57*, 531–538.
[23] E. Dova, R. Peschar, M. Sakata, K. Kato, A. F. Stassen, H. Schenk, J. G. Haasnoot, *Acta Crystallogr. Sect. B* **2004**, *60*, 528–538.
[24] E. Dova, R. Peschar, M. Takata, E. Nishibori, H. Schenk, A. F. Stassen, J. G. Haasnoot, *Chem. Eur. J.* **2005**, *11*, 5855–5865.
[25] Materials Studio. Accelrys Inc., 6985 Scranton Road, San Diego, CA 92121–3752, USA, **2001**.
[26] A. C. Larson, R. B. Von Dreele, General Structure Analysis System (GSAS), Los Alamos National Laboratory Report LAUR 86–748, **1994**.
[27] A. L. Spek, PLATON, Utrecht University, Utrecht (The Netherlands), **2001**.
[28] a) W. T. Pennington, *J. Appl. Crystallogr.* **1999**, *32*, 1028–1029; b) G. Cordier, *Nachr. Chem. Tech. Lab.* **1999**, *47*, 1437–1438.
[29] R. A. J. Driessen, B. O. Loopstra, D. P. de Bruijn, H. P. C. E. Kuipers, H. Schenk, *J. Comp.-aided Molec. Design* **1988**, *2*, 225–233.
[30] C. P. Slichter, H. G. Drickamer, *J. Chem. Phys.* **1972**, *56*, 2142–2160.
[31] S. Onishi, S. Sugano, *J. Phys. C* **1981**, *14*, 39–55.
[32] H. Spiering, E. Meissner, H. Köppen, E. W. Müller, P. Gütlich, *Chem. Phys.* **1982**, *68*, 65–71.
[33] M. Sorai, S. Seki, *J. Phys. Chem. Solids* **1974**, *35*, 555–570.
[34] H. Bolvin, O. Kahn, *Chem. Phys. Lett.* **1995**, *192*, 295–305.
[35] E. Dova, PhD Thesis, Amsterdam, The Netherlands, **2003**.
[36] S. Pillet, J. Hubsch, C. Lecomte, *Eur. Phys. J. B* **2004**, *38*, 541–552.
[37] J.-A. Real, B. Gallois, T. Granier, F. Suez-Panama, J. Zarembowitch, *Inorg. Chem.* **1992**, *31*, 4972–4979.
[38] E. Nishibori, M. Takata, K. Kato, M. Sakata, Y. Kubota, S. Aoyagi, Y. Kuroiwa, M. Yamakata, N. Ikeda, *Nucl. Instrum. Methods Phys. Res. Sect. A* **2001**, *467–468*, 1045–1048.
[39] J. W. Visser, *J. Appl. Crystallogr.* **1969**, *2*, 89–95.
[40] R. Peschar, unpublished results.
[41] V. B. Zlokazov, V. V. Chernyshev, *J. Appl. Crystallogr.* **1992**, *25*, 447–451.
[42] H. Toraya, *J. Appl. Crystallogr.* **1986**, *19*, 440–447.
[43] G. E. Engel, S. Wilke, O. Köning, K. D. M. Harris, F. J. J. Leusen, *J. Appl. Crystallogr.* **1999**, *32*, 1169–1179.
[44] R. A. J. Driessen, unpublished results.
[45] B. H. Toby, *J. Appl. Crystallogr.* **2001**, *34*, 210–213.
[46] H. D. Megaw, *Nature* **1934**, *134*, 900–901.

Received: December 20, 2005
Published online: April 27, 2006

